University College Dublin
An Coláiste Ollscoile, Baile Átha Cliath

School of Mathematics and Statistics
Scoil na Matamaitice agus Staitisticí
Experiments in Fluid Mechanics

For use in Advanced Fluid Mechanics (ACM 40890)

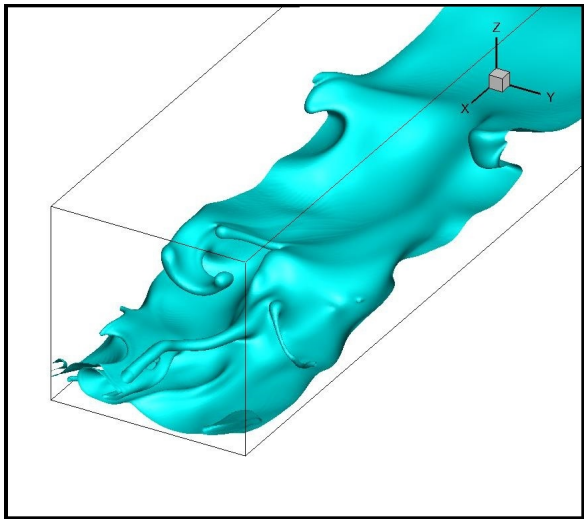

Dr Lennon Ó Náraigh

Lecture Notes in Fluid Mechanics
January 2025

Contents

1 Droplet-Impact Experiment **3**

2 Wave-Tank Experiment **10**

3 Turbulence Modelling **18**

Introduction

This handbook contains a list of combined experimental-theoretical-computational projects in Fluid Mechanics. The aim of these projects is to equip students who are interested in Fluid Mechanics to combine all three approaches, and hence to gain a complete picture of Fluid Mechanics. Lord Rayleigh, George Gabriel Stokes, and G. I. Taylor combined theory and experiment in their research. There are great stories of G. I. Taylor on board the Ice Patrol vessel *Scotia* making meteorological measurements, and then going downstairs to follow up his observations with theoretical modelling [BT96]. If these scientists were alive today, doubtless they would be doing simulations, on top of experiments and modelling.

This tradition is lost somewhat in modern Mathematics departments. The aim of these notes is to bring back this combination of different methods. There is also a very solid modern rationale for combining doing so, from both the scientific and pedagogic points of view. Indeed, this combination of methods will expose students to key methodologies in Fluid Mechanics, thus helping to make them into 'well rounded' scientists. By doing experiments in Fluid Mechanics, students will also gain marketable skills in data acquisition, image processing, and data postprocessing. With the advent of cheap cameras and the ease with which video can be postprocessed, this has become very easy to do. Hence, the rationale for the experiments (and and numerical simulations!) contained in this handbook.

Resources

The aim of these notes is to lay out a suite of projects which combine experimental measurement, theoretical modelling, and computer simulation. The experiments are carefully documented, as are the various pieces of theory needed. The theory can be read in conjunction with the lecture notes. For the computer simulation, the notes rely on the OpenFOAM software. To use this properly, students are invited to follow the tutorials of Joseph Nagy in the first instance:

- Installing OpenFOAM: `https://www.youtube.com/watch?v=cKyHFwfGpVQ&t=749s`
- Visualization: `https://www.youtube.com/watch?v=8J59CpaYnVc&t=2s`

- First Simulation: https://www.youtube.com/watch?v=KznljrgWSvo&t=758s
- Mesh Generation: https://www.youtube.com/watch?v=Ds0eK1wXMks&t=1203s
- Volume-of-Fluid Method: https://www.youtube.com/watch?v=gZ_TqsPwiXY
- Turbulence Modelling: https://www.youtube.com/watch?v=IPExwi2Ar-g

Chapter 1

Droplet-Impact Experiment

Overview

The focus of this project is droplet impact. A droplet is let fall from a height and impacts a solid surface. Roughly speaking, the fluid viscosity, the droplet velocity before impact, and and the surface properties (e.g., the contact angle) determine how far the droplet spreads after impact, and whether or not droplet splash occurs. The aim of this project is to make this statement precise. This will be achieved by carrying out a number of experiments where the Weber number is varied, with a view to validating correlations in the literature that predict the spreading radius as a function of these key parameters. Students will then be invited to compare the outcome of their experimental investigations with corresponding simulations using the OpenFOAM simulation software. The project is underpinned by a Github repository, created by past students:

`https://github.com/joeyanderson1/Droplet-Impact`

1.1 Context

When a droplet of fluid impacts on a surface, it spreads (and often rebounds) until it reaches an equilibrium configuration. At equilibrium, the angle between the liquid-gas interface and the solid surface is measured (conventionally, through the liquid), to yield the equilibrium contact angle θ_{eq}. If the angle is less than 90°, the substrate is deemed hydrophilic, whereas if the angle exceeds 90°, the substrate is deemed hydrophobic [dG85]. Droplet spreading then describes the dynamic phase after impact, but before the attainment of this equilibrium (e.g. Figure 1.1).

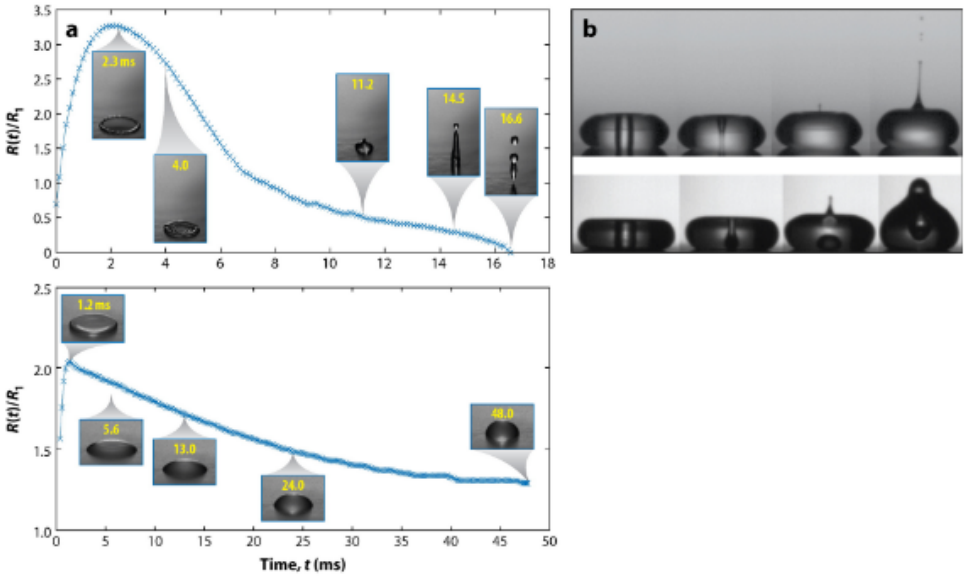

Josserand C, Thoroddsen ST. 2016.
Annu. Rev. Fluid Mech. 48:365–91

Figure 1.1: Snapshots of spreading and rebounding dynamics as well as the evolution of the spreading radius with time. Image taken from Reference [JT16].

This phenomenon has been studied intensely, due to its importance in industrial applications, including spray coating and painting, spray cooling, inkjet printing, and pesticide deposition on plant leaves [MLJ20]. Understanding droplet impact is also of key importance in forensic science [AMD+13]. A key problem in droplet impact studies is to determine the maximum extent $D_{\max}$ of the droplet, as a function of impact velocity, viscosity, and contact angle. In mathematical terms, the aim is to estimate the function f:

$$\frac{D_{\max}}{D_0} = f\left(\mathrm{We}, \mathrm{Re}, \theta\right), \tag{1.1}$$

where:

- D_0 is the diameter of the (spherical) droplet, prior to impact,
- $\mathrm{We} = \rho D_0 U_0^2/\sigma$ is the Weber number: U_0 is the droplet velocity prior to impact, ρ is the liquid density inside the droplet, and σ is the surface tension;
- $\mathrm{Re} = \rho D_0 U_0/\mu$ is the Reynolds number, μ is the viscosity of the liquid inside the droplet.
- θ is the contact angle, this is not necessarily the same thing as the equilibrium contact angle.

In this project, the students will theoretical, numerical, and experimental techniques to determine the function f in Equation (1.1).

1.2 Theoretical Techniques

A common method to estimate f is an energy-balance method. The initial energy E_{i} of the droplet prior to impact is surface energy and kinetic energy. Some of this energy is dissipated through viscous effects, for a total energy loss $\mathcal{D}$. The final energy E_{f} of the droplet at maximum extent is assumed to be purely surface energy. So, by energy conservation:

$$E_{\mathrm{i}} = \mathcal{D} + E_{\mathrm{f}}. \tag{1.2}$$

It is certainly straightforward to compute E_{i}. People then estimate $\mathcal{D}$ and E_{f} using various models, which has resulted in a proliferation of estimates for f in the literature. A standard approach in the literature [PFQCM96] is to use boundary-layer theory to estimate $\mathcal{D}$ and to estimate the final droplet at maximum extent as a cylinder, which gives

$$\mathcal{D} = \tfrac{1}{3}\pi\rho U_0^2 D_{\max}^2 D_0, \qquad E_{\mathrm{f}} = \tfrac{1}{4}\pi D_{\max}^2(1-\cos\theta_a), \tag{1.3}$$

where here, the *advancing contact angle* is used in the computation of the surface energy. By combining Equations (1.2)–(1.3), one obtains the following standard expression for $\xi_{\max} = D_{\max}/D_0$:

$$\xi_{\max} = \sqrt{\frac{\mathrm{We}+12}{3(1-\cos\theta_a)+4(\mathrm{We}/\sqrt{\mathrm{Re}})}} \tag{1.4}$$

1.3 Numerical Techniques

To model the droplet-impact problem numerically, it is necessary to solve the Navier–Stokes equations inside the liquid and the gas, and to match both sets of equations across the interface. At the same time, the interface separating the phases must be tracked using the kinematic condition. In practice, this difficult task is avoided by going over to a *one-fluid formulation*, where each phase is treated as different parts of a single fluid, with a density and viscosity profile that jumps sharply, depending on whether the region of interest is rich in one fluid phase or the other. A standard way of doing this is via a volume-of-fluid method, which we introduce briefly here. This was first introduced by Brackbill [BKZ92].

To develop a one-fluid formulation, a characteristic function is introduced:

$$\chi(\boldsymbol{x}) = \begin{cases} 1, & \text{if } \boldsymbol{x} \text{ is in phase 1,} \\ 0, & \text{if } \boldsymbol{x} \text{ is in phase 2,} \end{cases} \tag{1.5}$$

However, $\chi(\boldsymbol{x})$ is a step function, which has no place in a differential-equation-based model, which

requires the existence of smooth partial derivatives. Hence, one works with a locally-averaged volume fraction:

$$\alpha(\boldsymbol{x}) = \frac{1}{V}\int_V \chi(\boldsymbol{x})\mathrm{d}^3x, \tag{1.6}$$

where V is a small test volume. Correspondingly,

$$\rho(\boldsymbol{x}) = \rho_1\alpha(\boldsymbol{x}) + \rho_2(1-\alpha(\boldsymbol{x})), \tag{1.7}$$

and the same for the viscosity $\mu(\boldsymbol{x})$. Here, ρ_1 and ρ_2 are the constant densities of the individual phases. Also, α is referred to as the volume-of-fluid function.

As the volume-averaging in Equation (1.6) effectively smooths the interface between the phases, a continuous one-fluid equation of motion can now be written down:

$$\rho(\boldsymbol{x})\left(\frac{\partial \boldsymbol{u}}{\partial t} + \boldsymbol{u}\cdot\nabla\boldsymbol{u}\right) = -\nabla p + \nabla\cdot\left[\mu(\boldsymbol{x})\left(\nabla\boldsymbol{u} + \nabla\boldsymbol{u}^T\right)\right] - \rho(\boldsymbol{x})g\mathbf{k} + \boldsymbol{F}_{ST}. \tag{1.8}$$

For an incompressbile fluid, the conservation of mass of the different phases now reduces to:

$$\frac{\partial\alpha}{\partial t} + \boldsymbol{u}\cdot\nabla\alpha = 0, \qquad \nabla\cdot\boldsymbol{u} = 0. \tag{1.9}$$

In the foregoing equations, $\boldsymbol{F}_{ST}$ is the surface-tension force. In the sharp-interface formulation, this would be:

$$\boldsymbol{F}_{ST} = \sigma\mathbf{n}\kappa\delta(\boldsymbol{x}-\boldsymbol{x}_I), \tag{1.10}$$

where σ is the surface tension, $\mathbf{n}$ is the unit normal to the interface, κ is the mean curvature, and $\boldsymbol{x}_I$ is the instantaneous interface location. The delta function is zero everywhere except at the interface location $\boldsymbol{x} = \boldsymbol{x}_I$. This can be re-written as $\delta(\boldsymbol{x}-\boldsymbol{x}_I) = |\nabla\alpha|\delta(\alpha-(1/2))$. Similarly,

$$\widehat{\boldsymbol{n}} = \left(\frac{\nabla\alpha}{|\nabla\alpha|}\right)_{\alpha=1/2}. \tag{1.11}$$

As the curvature is given by $\kappa = -\nabla\cdot\widehat{\boldsymbol{n}}$, this gives:

$$\boldsymbol{F}_{ST} = -\sigma\left[\nabla\alpha(\nabla\cdot\widehat{\boldsymbol{n}})\right]_{\alpha=1/2}. \tag{1.12}$$

Now, for the purpose of solving Equation (1.8), the volume-of-fluid method distributes this force over the entire volume:

$$\boldsymbol{F}_{ST} \approx -\sigma\left[\nabla\alpha(\nabla\cdot\widehat{\boldsymbol{n}})\right], \tag{1.13}$$

This is a good approximation, because $\alpha \approx \text{Const} = 1$ or 0 away from the interface. Of course, the approximation does lead to notorious spurious currents [SSÓ NáraighA17].

Boundary conditions on Equation (1.8) are standard no-slip conditions – except when the contact line intersects the boundary ($= \partial\Omega$). In that case, the gradient of α at the contact line has to me adjusted to match the contact angle [BKZ92]. To allow for contact-line motion, it is standard to prescribe a slip boundary condition:

$$u = \lambda \left(\frac{\partial u}{\partial z} \right), \qquad \text{at } z = 0. \tag{1.14}$$

Here, we have used (conventionally) u for a velocity component tangent to the wall, and z for the wall-normal direction. The constant λ is the slip length. The slip length is a physical quantity, however it is $O(\mathrm{nm})$, which can't be resolved in a standard numerical simulation. Hence, it is customary to make λ much larger than this, or simply to set the slip length to zero, and to 'allow the triple point to slip via numerical diffusion'.

A final ingredient in the volume-of-fluid simulations is a model for the dynamic contact angle:

$$\theta(t) = f(\theta_e, U, ...). \tag{1.15}$$

where, U is the contact-line velocity – sometimes taken in a computational model to be the tangential velocity in the cell nearest to the contact line. In OpenFOAM, a very simple contact-angle model is available:

$$\theta(t) = \theta_e + (\theta_a - \theta_r) \tanh(U/U_\theta). \tag{1.16}$$

This allows for contact-angle hysteresis – which is the possibility that for the surface under consideration, we have $\theta_a > \theta_r$ (advancing and receding contact angles, respectively). In this context, θ_e stands for the equilibrium or static contact angle, which is the classic contact angle that a stationary sessile drop makes with the surface. Finally, int his model U_θ is a model parameter. Equation (1.16) is highly simplistic. The model that is deemed most accurate and up to date is due to Kistler [GMSE18].

1.4 Experimental Techniques

There is no 'universal' formula for f. The model in Equation (1.4) gets the basics right but details are missing. The details can be filled in with either numerical simulations or experiments, or preferably both. In fact, for this problem, both are needed. The direct numerical simulations have drawbacks because an extremely high resolution is required, as well as a model for the slip, or the relative motion of the contact line with respect to the surface (the standard no-slip condition on the Navier–Stokes equations is not appropriate here). Experiments can guide us in the selection of the right slip-length model. On the other hand, the experiments have their drawbacks because it is difficult to visualize

the flow inside the droplet on the relevant timescale (ms). Direct numerical simulations are an excellent way to visualize the flow inside the droplet – and hence, to perfect the dissipation model in Equation (1.3). Thus, to understand this problem fully, a combination of theoretical modelling, experimental techniques, and direct numerical simulation is required.

1.5 The Project

Using the experimental rig in Figure 1.2 and the Chronos 1.4 high-speed camera:

`https://www.krontech.ca/product/chronos-1-4-high-speed-camera/`

plan out and execute a droplet-impact experiment. Some things to bear in mind:

- What are the standard lengthscales and velocity scales in the experimental problem. How can these be measured? Hint: Your mobile phone and a ruler will come in handy here.
- For a fixed working fluid, what dimensionless parameter can be varied? How can this be varied to validate Equation (1.4)?
- The droplet-splash threshold parameter is often given in the literature as $K = \mathrm{WeRe}^{1/2}$, with $K \lesssim 3,000$ for splash to be avoided [JT16]. In your experiment, why might it be important to keep K below this threshold value?
- What is the appropriate value of the contact angle for use in Equation (1.4)? Hint: Use postprocessing of your videos and the python code:

  `https://github.com/joeyanderson1/Droplet-Impact/tree/main/Joseph/Python_Code`

  to estimate the dynamic contact angle.

Students should finally compare the results of say one experimental run with an OpenFOAM simulation, case files for which can be downloaded from the repository.

Figure 1.2: Droplet-impact experiment

Chapter 2

Wave-Tank Experiment

Overview

The focus of this project is waver waves, where both gravity and surface tension play a role. Students will use a wavemaker in small-scale wave tank to generate capillary waves at a particular frequency. The students will then measure the wavelengths of the wave formed in the tank with mobile-phone video analysis. This will provide an opportunity to examine in detail the dispersion relation

$$\omega^2 = k\left(g + \frac{\sigma}{\rho}k^2\right)\tanh(kh), \tag{2.1}$$

valid for water waves in a finite depth, under the assumption of inviscid flow. Here, in standard notation,

- ω is the frequency of the wave;
- k is the wavenumber;
- g is acceleration due to gravity;
- σ is surface tension;
- ρ is the density of liquid;
- h is the depth of the undisturbed liquid.

Finally, students will explore – using OpenFOAM software – to what extent the water waves in the tank can be modelled using Computatioinal Fluid Dynamics.

2.1 Context

The dispersion relation (2.1) is derived from linear water-wave theory. Some of the details are provided below in Section 2.2, the rest can be filled in by an interested reader. The fundamental

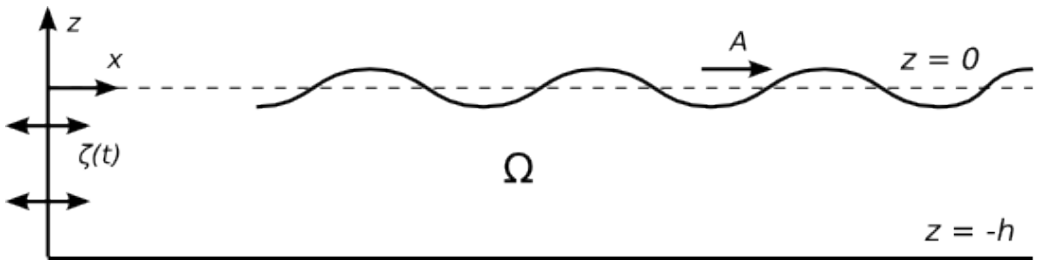

Figure 2.1: Schematic description of the wave-maker. Taken directly from the website [Wav]

assumption is that the fluid is inviscid and irrotational, meaning that inside the domain, the flow has a velocity potential Φ which satisfies Laplace's equation. Appropriate boundary conditions are then applied. These depend on time, and this introduces the necessary time-dependence to derive a dispersion relation such as Equation (2.1). The overall approach is similar to the one used in the Lecture Notes for deriving the dispersion relation for the Rayleigh–Taylor instability (in the inviscid case), or the Kelvin–Helmholtz instability. However, a point of departure is that in the present case, the interfacial waves are linearly stable.

Linear water wave theory finds many applications in understanding the ocean waves, both from a fundamental scientific point of view (for instance, characterizing the wave spectrum), as well as from a coastal engineering perspective. The basic theory outlined in here assumes a flat bottom topography. Many interesting wave phenomena can occur when the bottom topography is something other than flat. For instance, wave refraction occurs on a sloping beach. Similarly, the water-wave theory presented in here is based on a linearization of the dynamics. This is a good approximation in deep water, far out to sea. It is not such a good approximation on a beach, where wave breaking occurs. For this reason, the investigation in this chapter should be viewed as a first foray in to water-wave theory.

2.2 Theoretical Formulation

This section is taken mainly from Reference [Wav], with the necessary modifications being made herein to describe gravity-capillary (as opposed to pure gravity) waves. Refer to Figure 2.1 for the setup. A paddle at location $x = 0$ oscillates according to:

$$\xi(z,t) = \Re\left[-\frac{1}{\mathrm{i}\omega} f(z)\mathrm{e}^{-\mathrm{i}\omega t}\right]. \tag{2.2}$$

where $f(z)$ is a shape function describing the details of the back-and-forth motion of the paddle. This can be left unspecified for now.

Inside the domain Ω, the flow is inviscid and irrotational, so potential theory applies:

$$\nabla^2\Phi = 0, \qquad \boldsymbol{x} \in \Omega. \tag{2.3}$$

Here, Φ is the velocity potential, such that $\boldsymbol{u} = \nabla\Phi$. The amplitude of the surface waves is assumed to be small, so that the domain of the liquid can be linearized on to:

$$\{(x, z)| - h < z < 0\, x > 0\}.$$

We henceforth take this to be the domain Ω. The boundary condition at $z = -h$ is the no-penetration condition, $w = 0$, hence:

$$\frac{\partial\Phi}{\partial z} = 0, \qquad z = -h. \tag{2.4}$$

2.2.1 Interfacial conditions

We next look at the boundary condition at $z = 0$. Bernoulli's equation gives the pressure in Ω as:

$$p = -\rho\frac{\partial\phi}{\partial t} - \tfrac{1}{2}\rho\boldsymbol{u}^2 - \rho g\eta + c(t), \tag{2.5}$$

where η is the interface height (assumed small), and $c(t)$ is a parameter associated with Bernoulli's principle. For a steady flow, this would be a simple constant of integration. The standard jump condition at the interface is:

$$[\![p]\!] = \sigma\kappa, \tag{2.6}$$

where κ is the curvature, hence:

$$[\![p]\!] = \sigma\eta_{xx}. \tag{2.7}$$

By identifying the jump in pressure as $p - p_{atm}$, we combine the previous expressions as:

$$p - p_{atm} = -\rho\frac{\partial\phi}{\partial t} - \tfrac{1}{2}\rho\cancel{\boldsymbol{u}^2} - \rho g\eta + c(t) - p_{atm} = -\sigma\eta_{xx}, \qquad z = 0. \tag{2.8}$$

Here, the term $(1/2)\rho\boldsymbol{u}^2$ is neglected because of the small-amplitude approximation. Furthermore, by choosing $c(t) = p_{atm}$, to further terms drop out, leaving:

$$-\rho\frac{\partial\Phi}{\partial t} + \rho g\eta - \sigma\eta_{xx}. \tag{2.9}$$

We now make the standard transformations:

$$\begin{aligned}\Phi &= \Re\left[\phi(\boldsymbol{x})\mathrm{e}^{-\mathrm{i}\omega t}\right],\\ \eta &= \Re\left[\widehat{\eta}\mathrm{e}^{-\mathrm{i}\omega t}\right].\end{aligned}$$

However, we will use Φ and ϕ interchangeably, and the same for η and $\widehat{\eta}$, as the context will determine which variable is being used. In this way, Equation (2.9) becomes:

$$\rho \mathrm{i}\omega = \rho g\eta - \frac{\sigma}{\rho}\eta_{xx}, \qquad z = 0. \tag{2.10}$$

A second interfacial condition is the kinematic condition. In the small-amplitude approximation, this is $\eta_t = w$, or $\eta_t = \Phi_z$, hence:

$$-\mathrm{i}\omega\eta = \frac{\partial\phi}{\partial z}, \qquad z = 0. \tag{2.11}$$

We combine Equations (2.10)–(2.11). First, Equation (2.11) gives $\eta = -1/(\mathrm{i}\omega)\phi_z$. We substitute this into Equation (2.10) to obtain a single boundary condition at $z = 0$:

$$\omega^2\phi = g\frac{\partial\phi}{\partial z} - \frac{\sigma}{\rho}\partial_{xx}\frac{\partial\phi}{\partial z}, \qquad z = 0. \tag{2.12}$$

2.2.2 Solving Laplace's Equation

We solve $\nabla^2\phi = 0$ in Ω. We do separation of variables to get $\phi(x, z) = X(x)Z(z)$. Following standard steps, we get:

$$\frac{X''}{X} = -\frac{Z''}{Z} = k^2. \tag{2.13}$$

We look at the boundary conditions at $z = 0$ next. The boundary condition (2.12) gives:

$$\omega^2 X(x)Z(0) = \left(gX(x) - \frac{\sigma}{\rho}X''(x)\right)Z'(0). \tag{2.14}$$

We use the separation-of-variables condition (2.13) to reduce this to:

$$\omega^2 Z(0) = \left(g - \frac{\sigma}{\rho}k^2\right)Z'(0). \tag{2.15}$$

We further re-write this as:

$$Z'(0) = \alpha_k Z(0), \qquad \alpha_k = \frac{\omega^2}{g - \frac{\sigma}{\rho}k^2}. \tag{2.16}$$

Putting it all together, we have to solve:

$$\begin{aligned} Z'' + k^2 Z &= 0, && \text{(2.17a)} \\ Z'(-h) &= 0, && \text{(2.17b)} \\ Z'(0) &= \alpha_k Z(0). && \text{(2.17c)} \end{aligned}$$

The solution is:

$$Z = \frac{\cos[k(z+h)]}{\cos kh}, \tag{2.18}$$

with solvability condition $k\tan(kh) = -\alpha_k$, or:

$$k\tan(kh) = -\frac{\omega^2}{g - \frac{\sigma}{\rho}k^2}. \tag{2.19}$$

We label the solutions of Equation (2.20) as k_n, where $n \in \{0, 1, 2, \cdots\}$.

2.2.3 Dispersion Relation

Equation (2.19) has two solution types:

- Case 1. This corresponds to $n = 0$, so we are dealing with k_0. In this case, k_0 is purely imaginary, and we write $k_0 = \pm \mathrm{i}\kappa$, where κ is real. Using the properties of trigonometric functions, Equation (2.20) reduces to:

  $$\kappa\tanh(\kappa h) = \frac{\omega^2}{g + \frac{\sigma}{\rho}\kappa^2}, \tag{2.20}$$

  which is precisely Equation (2.1). In this case, however, ω is known, and κ has to be obtained by inversion. A sample dispersion curve is shown in Figure 2.2.

- Case 2. In this case, we look at k_n, where $n \geq 1$. A standard graphical eigenvalue analysis shows in this case there are infinitely many real positive roots, confirming that $n \in \{1, 2, \cdots\}$.

Putting the two cases together, we have the following set of eigenfunctions, with $Z(z) \to \chi_n(z)$:

$$\chi_n(z) = \begin{cases} \frac{\cos[k_n(z+h)]}{\cos k_n h}, & n \geq 1 \\ \frac{\cosh[\kappa(z+h)]}{\cosh \kappa h}, & n = 0. \end{cases} \tag{2.21}$$

As these are eigenfunctions of a self-adjoint operator, we have an orthogonality relation

$$\int_{-h}^{0} \chi_m(z)\chi_n(z)\mathrm{d}z = A_n \delta_{nm}. \tag{2.22}$$

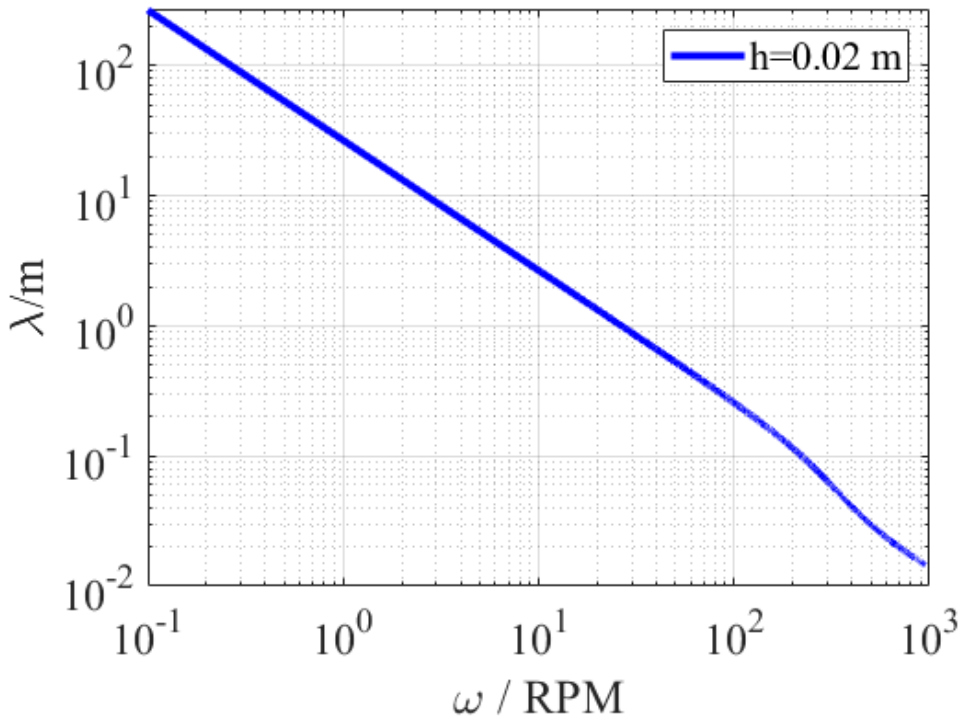

Figure 2.2: The dispersion relation (2.20). For a given ω, there is a uniquely determined k-value, hence a uniquely determined wavelength $\lambda = 2\pi/k$.

2.2.4 General Solution

The general solution for the velocity potential can now be written as:

$$\phi(x,z) = \sum_{n=1}^{\infty} a_n \chi_n(z) \mathrm{e}^{-k_n x} + a_0 \chi_0(z) \mathrm{e}^{-\mathrm{i}\kappa x}. \tag{2.23}$$

Notice that we do not allow for a contribution proportional to $\mathrm{e}^{\mathrm{i}\kappa x}$, as this would correspond to a wave travelling inward from positive infinity, which is not physical [1]. Furthermore, at $x = 0$, we have:

$$\left(\frac{\partial \phi}{\partial x}\right)_{(x=0,z)} = \sum_{n=1}^{\infty} a_n \chi_n(z)(-k_n) + a_0 \chi_0(z)(\mathrm{i}\kappa). \tag{2.24}$$

A boundary condition at $x = 0$ would be $\partial_x \phi = u = \partial_t \xi$, where ξ is the displacement of the wall at $x = 0$ (*cf.* Equation (2.2)). Thus, we obtain:

$$\sum_{n=1}^{\infty} a_n \chi_n(z)(-k_n) + a_0 \chi_0(z)(\mathrm{i}\kappa) = f(z). \tag{2.25}$$

[1] This is the so-called Sommerfeld Radiation Condition.

Hence, the coefficients a_0 and a_n can be determined from:

$$\begin{aligned} a_0 &= -\frac{1}{(-\mathrm{i}\kappa)A_0}\int_{-h}^{0} f(z)\chi_0(z)\mathrm{d}z, \\ a_n &= -\frac{1}{k_n A_0}\int_{-h}^{0} f(z)\chi_0(z)\mathrm{d}z, \qquad n \geq 1. \end{aligned}$$

Crucially, in the far field, we have

$$\phi \sim a_0\chi_0(z)\mathrm{e}^{-\mathrm{i}\kappa x}, \qquad x \to \infty, \tag{2.26}$$

since $\mathrm{e}^{-k_n x} \to 0$ as $x \to \infty$, for $n \geq 1$. These waves that give no contribution in the far field are called **evanascent**. Only the oscillatory wave with dispersion relation (2.20) survives far downstream of the disturbance.

2.2.5 Results

By analysing the dispersion relation (2.20), we can see what type of wavelengths can be expected for a given forcing frequency. The wavelengths depend sharply on depth, as shown in Table 2.1.

ω (RPM)	λ ($h = 0.08\,\mathrm{m}$)	λ ($h = 0.02\,\mathrm{m}$)
10	5.29	2.65
50	1.02	0.526
100	0.452	0.256
200	0.142	0.115

Table 2.1: Expected wavelengths (in metres), based on the dispersion relation (2.20). Here, we have used $g = 9.8\,\mathrm{m}\cdot\mathrm{s}^{-2}$ and $\sigma = 0.072\,\mathrm{N}\cdot\mathrm{m}^{-1}$.

2.3 Numerical Techniques

The volume-of-fluid method introduced in Chapter 1 can be used to model the waves in a wave tank. The volume-of-fluid method usually solves the full Navier–Stokes equations in both phases with the effect of viscosity included (for instance, `interFOAM` in OpenFOAM). However, the difference between this complete description of the motion, and the approximate description given by potential flow, is small for water waves. Hence, it should be possible to validate the dispersion relation (2.1) (derived in the case of potential flow) using the full Navier–Stokes equations for both fluid phases.

2.4 The Project

Using the experimental rig in Figure **??** and mobile-phone video analysis, plan out and execute an experiment to test the dispersion relation (2.1).

- What parameters can be varied?
- What are realistic wavelengths for the tank under investigation? How can such wavelengths be achieved?
- What are the boundary conditions at the tank end? How might this impact the experiment?
- Can the surface tension be varied? How might this add additional insights to the project?

Students should finally compare the results of say one experimental run with an OpenFOAM simulation. A complete OpenFOAM model of a numerical wave tank can be found here:

`https://olaflow.github.io/`

In particular, the two-dimensional flume is most relevant to the present experiment:

`https://github.com/phicau/olaFlow/tree/master/tutorials/baseWaveFlume`

Chapter 3

Turbulence Modelling

Overview

This chapter is a computational project. The aim is to compare the simulation results in the typed notes on turbulence, with an OpenFOAM implementation of the same set-up. The main thing students will learn in this project is how to map a model which uses dimensionless variables to a model which uses dimensional ones.

3.1 First Part

Following the typed notes, obtain sTPLS with the large-eddy simulation from the repository. Configure and compile a version on whatever multicore machine you can find. Run the code for a sufficeint length o ttime to generate turbulent statistics. Plot the average streamwise turbulent velocity field and compare the results for the bulk flow with prior work from the literature.

3.2 Second Part

In this second part, we will compare the results of the First Part with a corresponding OpenFOAM simulation. Because OpenFOAM uses dimensional variables, we will look at a simulation domain that is $1\,\mathrm{m}$ high, $8\,\mathrm{m}$ long, and $4\,\mathrm{m}$ wide. Correspondingly, the density should be set to $1\,\mathrm{kg/m^3}$. If the Reynolds number in the First Part was Re_*, then the kinematic viscosity should now be set to $\mathrm{Re}_*^{-1}\,\mathrm{m}\cdot\mathrm{s}^{-2}$.

We impose periodic boundary conditions in the x-direction, to map on to the First Part. Hence, the

pressure field (in the notation given in the typed notes) is:

$$q(\boldsymbol{x}, t) = p(\boldsymbol{x}, t) - |\mathrm{d}P/\mathrm{d}L|x.$$

Here, $p(\boldsymbol{x}, t)$ has the periodic boundary conditions in the x-direction, and the constant pressure drop $|-\mathrm{d}P/\mathrm{d}L|$ drives the flow in the x-direction. To introduce this constant driving force into the OpenFOAM simulation, it suffices to set the gravity vector to be in the negative x-direction, and to have magnitude 1. Hence, we make the identification

$$g_x \to -|\mathrm{d}P/\mathrm{d}L|.$$

The reason this works is because:

$$\nabla q = \nabla p \underbrace{-|\mathrm{d}P/\mathrm{d}L|\widehat{\boldsymbol{e}}_1}_{=g_x}.$$

Hence, a gravity force in the x-direction plays the same role as a constant pressure drop.

3.2.1 Other issues

Students will have to investigate whether a uniform mesh with wall functions is sufficient to reproduce the turbulence simulation from the First Part.

Bibliography

[AMD+13] Daniel Attinger, Craig Moore, Adam Donaldson, Arian Jafari, and Howard A Stone. Fluid dynamics topics in bloodstain pattern analysis: comparative review and research opportunities. *Forensic science international*, 231(1-3):375–396, 2013.

[BKZ92] Jeremiah U Brackbill, Douglas B Kothe, and Charles Zemach. A continuum method for modeling surface tension. *Journal of computational physics*, 100(2):335–354, 1992.

[BT96] George Keith Batchelor and Geoffrey Ingram Taylor. *The life and legacy of GI Taylor*. Cambridge University Press, 1996.

[dG85] Pierre-Gilles de Gennes. Wetting: statics and dynamics. *Reviews of modern physics*, 57(3):827–863, 1985.

[GMSE18] Johan Göhl, Andreas Mark, Srdjan Sasic, and Fredrik Edelvik. An immersed boundary based dynamic contact angle framework for handling complex surfaces of mixed wettabilities. *International Journal of Multiphase Flow*, 109:164–177, 2018.

[JT16] Christophe Josserand and Sigurdur T Thoroddsen. Drop impact on a solid surface. *Annual review of fluid mechanics*, 48:365–391, 2016.

[MLJ20] Sara Moghtadernejad, Christian Lee, and Mehdi Jadidi. An introduction of droplet impact dynamics to engineering students. *Fluids*, 5(3), 2020.

[PFQCM96] M Pasandideh-Fard, YM Qiao, Sanjeev Chandra, and Javad Mostaghimi. Capillary effects during droplet impact on a solid surface. *Physics of fluids*, 8(3):650–659, 1996.

[SSÓ NáraighA17] Zlatko Solomenko, Peter DM Spelt, Lennon Ó Náraigh, and Pascal Alix. Mass conservation and reduction of parasitic interfacial waves in level-set methods for

the numerical simulation of two-phase flows: a comparative study. *International Journal of Multiphase Flow*, 95:235–256, 2017.

[Wav] `https://wikiwaves.org/Wavemaker_Theory`. Accessed: (13th September 2024).